THE ASTROPHYSICAL JOURNAL, 440:80–90, 1995 February 10

ULTRAVIOLET SPECTROPOLARIMETRY OF HIGH-REDSHIFT QUASARS WITH THE *HUBBLE SPACE TELESCOPE*[1]

C. D. IMPEY
Steward Observatory, University of Arizona, Tucson, AZ 85721
MATTHEW A. MALKAN AND WAYNE WEBB
Department of Astronomy, University of California, Los Angeles, CA 90024
AND
C. E. PETRY
Steward Observatory, University of Arizona, Tucson, AZ 85721
Received 1994 May 18; accepted 1994 August 26

ABSTRACT

Ultraviolet spectropolarimetry of three bright high-redshift low-polarization quasars (LPQs) was obtained with the Faint Object Spectrograph of the *Hubble Space Telescope*. Two of the quasars, PG 1634+706 and PG 2302+029, had polarizations $p \sim 0.5\%$–1.0% throughout the ultraviolet, and showed no significant variation of polarization amplitude or position angle with wavelength. PG 2302+029 was also marginally (2.4 σ) circularly polarized in the optical continuum. For the highest redshift quasar, PG 1222+228 (Ton 1530), the polarization was measured down to rest wavelengths below 800 Å. Although the continuum of PG 1222+228 was weakened by Lyman limit absorption from an intergalactic gas cloud, the polarization increased sharply from 1% to about 4.5%, a change of 4 σ significance. This abrupt rise in polarization does not appear attributable to any known instrumental artifact.

These UV polarizations were only slightly less than those previously observed for these same objects in the optical. The polarization spectra were flat with a typical slope of the polarized flux $pF_\nu \propto \nu^{-0.8\pm0.5}$. Unlike the case of several high luminosity Seyfert 1 nuclei studied previously, polarization caused by scattering from dust grains does not provide the best fit to the polarization spectra of these luminous quasars. The hypotheses that the polarization in these quasars is produced by transmission through aligned interstellar grains (in the Milky Way or the host galaxy), or by a synchrotron power-law component, appear to be ruled out. These observed spectra are consistent with a wavelength-independent polarization proportional to the total nonstellar light or, possibly, to the contribution of the blue thermal component.

The polarization spectra have insufficient signal-to-noise to locate the scatterers with respect to the continuum source and the much larger broad line region. A decrease in amplitude and rotation of the position angle of the polarization vector at the shortest wavelengths, which could result from general relativistic effects near a spinning black hole, was not observed. In fact, in PG 1222+228, the polarization was observed to increase at the shortest wavelengths. The rise in polarization with frequency is so sharp that it cannot be due to any *wavelength-independent* polarizing mechanism at any radius in an accretion disk. Such a rise could be attributable, for example, to a relative increase in scattering opacity over absorption at higher frequencies.

Subject headings: polarization — quasars: general — radiation mechanisms: nonthermal — ultraviolet: galaxies

1. INTRODUCTION

Spectropolarimetry is a powerful diagnostic tool for studying the continuum and line emitting regions of the variety of active galactic nuclei (AGNs). The dominant polarization observed in blazars from millimeter to ultraviolet wavelengths, for example, is believed to originate from a single, beamed, synchrotron component (Landau et al. 1986; Impey & Neugebauer 1988; Bregman 1990). In other types of active galaxies, the polarization is lower ($p \leq 1\%$), and its interpretation is more difficult. Among radio galaxies and Seyfert galaxies, there is a vigorous debate on the relative importance of polarization from: transmission through aligned dust grains, dust scattering, and electron scattering (Miller & Goodrich 1990; Cimatti et al. 1993; Antonucci 1992, 1993). In many cases the interpretation is complicated by the effects of dilution from an underlying host galaxy. The polarization position angle is usually independent of wavelength, suggesting that the polarization in a given object originates in a single physical progress. Depending on the polarization of the emission lines and the continuum, the scatterers are believed to be located near one of the following: the continuum region (sub-parsec scales), the broad line region (parsec scales), or the narrow line region (kiloparsec scales).

The degree of continuum polarization in normal quasars is generally low, with a weak tendency to increase toward shorter wavelengths (Stockman, Moore, & Angel 1984; Mead et al. 1990). These low levels of polarization, combined with the faintness of the sources, has resulted in little data being published. Webb et al. (1993), hereafter WMSI, made broadband polarization measurements through *U*, *B*, *V*, *R*, and *I* filters of 15 bright quasars. They compared the results with

[1] Based on observations with the NASA/ESA *Hubble Space Telescope*, obtained at the Space Telescope Science Institute, which is operated by the Association of Universities for Research in Astronomy, Inc., under NASA contract NAS 5-26555.

several models for the origin of the polarized flux. The different models included synchrotron emission, scattering from electrons or different types of dust grains, transmission through aligned grains, and scattering from electrons in an accretion flow. In 9 of the 15 quasars studied, the polarization was best understood as scattering from dust grains. These objects tended to be redder and, in several cases (e.g., Mkn 486), had broad emission lines which showed the same polarization as the continuum. For three objects, the best fit to the data was a model with polarization proportional to the flux of the blue thermal component. These latter objects tended to have lower levels of polarization and unpolarized (where measured) broad emission lines.

Differentiating between the different models for the origin of polarization can best be accomplished with data spanning a wide range of wavelengths. Polarimetry of high-redshift quasars is particularly desirable because the degrees of polarization predicted by the different models diverge in the ultraviolet.

2. OBSERVATIONS

Quasars selected for observation with the *Hubble Space Telescope* (*HST*) were chosen for their high redshifts, brightness, and measurable polarization at optical wavelengths.The high redshifts ensured that the continuum polarization could be measured far into the rest-frame ultraviolet. All three quasars have strong ultraviolet excesses, and existing high accuracy ground-based polarimetry [$\sigma(p) = 0.1\%$–0.2%]. PG 1222+228 has a radio power in excess of 10^{26} W Hz^{-1}; the other two have been detected at 8 GHz but are in the range of radio power generally referred to as radio-quiet (Kellerman et al. 1989). The three quasars and their properties are listed in Table 1, along with a summary of the observations.

Ultraviolet spectropolimetry of PG 1222+228, PG 1634+706, and PG 2302+029 was made with the Faint Object Spectrograph (FOS) of the *HST* on 1991 November 11–12, 1992 July 23–24, and 1992 July 28 (UT), respectively. All three quasars were observed with the G270H grating, which gives coverage from about the atmospheric cutoff down to 2200 Å. PG 1222+228 and 1634+706 were also observed with the G190H grating covering from 2300 down to 1600 Å. The continuum fluxes of these two quasars are strongly suppressed by optically thick intergalactic Lyman limit absorbers at wavelengths below 2320 and 1820 Å, respectively. PG 2302+029 was not observed with G190H for lack of time. The approximate dispersion for G270H is 0.52 Å per pixel and for G190H is 0.37 Å per pixel. All observations used the blue Digicon detector. Total integration times were 14400 s (G190H) and 12960 s (G270H) for PG 1222+228, 5280 s (G190H) and 5280 s (G270H) for PG 1634+706, and 7920 s (G270H) for PG 2302+029.

TABLE 1

DETAILS OF THE OBSERVATIONS

Properties	PG 1222+228	PG 1634+706	PG 2302+029
Redshift	2.046	1.334	1.044
V-magnitude	15.5	14.9	16.0
M_B[a]	−29.9	−29.6	−27.9
P_{radio} (W Hz^{-1})[b]	1.9×10^{26}	1.6×10^{25}	1.8×10^{24}
Date of observation	1991 Nov 11–12	1992 Jul 23–24	1992 Jul 28
HST/FOS gratings	G270H/G190H	G270H/G190H	G270H
Integration times (s)	14400/12960	5280/5280	7920

[a] Luminosities calculated for $H_0 = 50$ km^{-1} Mpc^{-1}, $q_0 = 0.5$.
[b] Radio luminosity from Kellerman et al. 1989.

The FOS serves as a polarimeter by rotating a waveplate/Wollaston prism combination into the beam just behind the entrance apertures. These observations used the *B* waveplate which is optimized for observations at ultraviolet wavelengths. The polarimeter has been described by Allen & Angel (1982), and calibrations are given by Allen & Smith (1992). A polarization observation consists of eight integrations at different positions of the waveplate; each polarization observation was completed within a particular orbit. Each target was acquired using an FOS binary search in a 4.3 arcsecond square aperture, and polarimetry was carried out using the same aperture. While this aperture allows almost all of the light from the aberrated (pre-COSTAR) *HST* images to enter the instrument, only 55% of the photoelectron image of the source is actually sampled by the diode array in the Digicon. Since Allen et al. (1993) have shown that the instrumental polarization of the FOS polarimeter is under 0.1%, it will be neglected in what follows.

Instrumental effects were removed from the data using a program written by Richard Allen of the FOS Instrument Team. A correction was made for dead diodes and the spectra were scaled to counts per second per pixel. The sky contribution was sufficiently small that sky subtraction was not required; however, a low level of instrumental background noise was subtracted. The data were flat fielded, then flux calibrated through multiplication by an inverse sensitivity function, and then wavelength calibrated. The retardation coefficients, Wollaston angles, and the waveplate angles were combined with a least squares fit to the data points at each waveplate position to produce the Stokes parameters.

The data from each of the two Digicon *y*-steps were then merged and a correction was made for the variation with wavelength of the position of the fast axis of the waveplate. Lastly, the resultant Stokes parameter values were averaged over broad wavelength bins due to the low polarization and the faint signal. Values of linear polarization have been corrected in all cases for the bias that results at low signal-to-noise levels (Wardle & Kronberg 1974). Tests showed that the resulting error bars were statistically well-behaved, in the sense of decreasing with the square root of the number of channels averaged. Field star polarimetry is available only for PG 1222+228, from WMSI. Since the interstellar polarization close to the line-of-sight is very small ($<0.3\%$), and its wavelength dependence in the ultraviolet is poorly known, no correction for interstellar polarization is made in this paper.

Although our motivation was spectropolarimetry, these high signal-to-noise observations produced high quality ultraviolet spectra of the three quasars. In a subsequent paper, we will consider these spectra, which cover the line-rich region of the Lyman-alpha "forest" in two quasars. Here we present the *HST* spectropolarimetry, and combine it with ground-based spectroscopy and polarimetry, in an attempt to constrain models for the origin of the polarized flux.

2.1. *Spectropolarimetry*

The measured polarizations were low and wavelength-independent, with the exception of PG 1222+228 in the extreme ultraviolet. Table 2 gives a summary of the ultraviolet polarimetry, with the Stokes parameters and derived values of

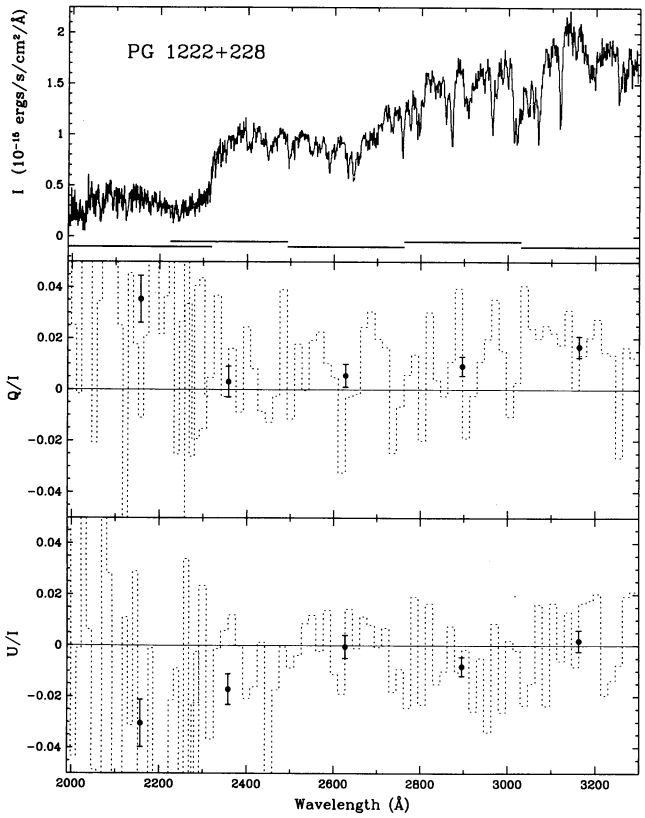

FIG. 1*a*

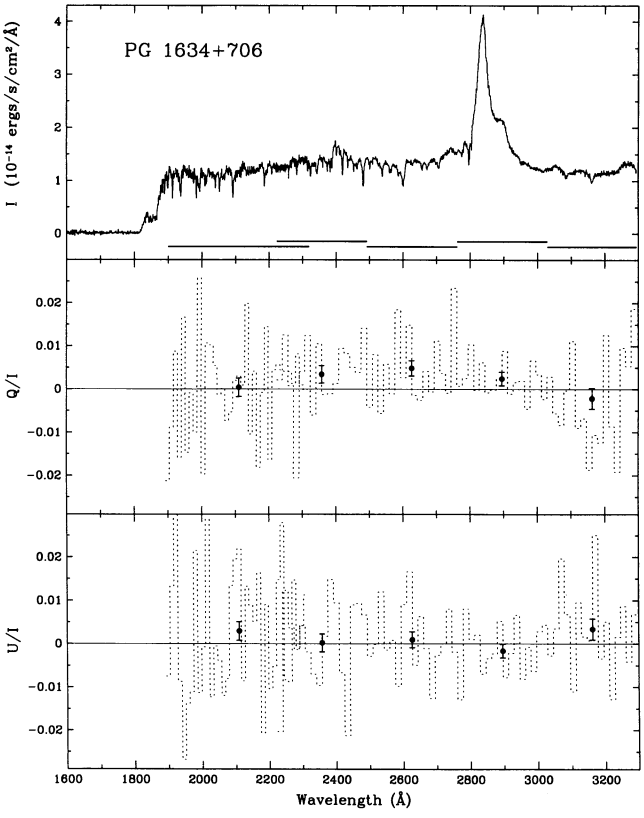

FIG. 1*b*

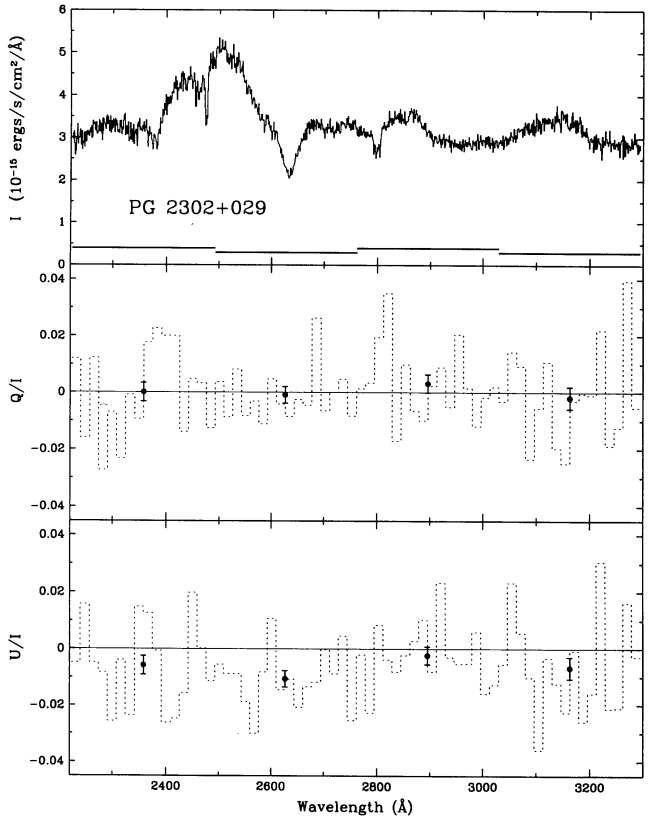

FIG. 1*c*

polarization and position angle calculated in broad wavelength bins. Figure 1*a*–1*c* shows the total intensity I, and the normalized Stokes parameters Q/I and U/I in adjacent vertical panels for each quasar. The total intensity is binned by two pixels for each quasar. The light dashed lines show Stokes parameters binned by 32 pixels, which corresponds to 16.6 Å for the G270H grating and 11.5 Å for the G190H grating. The filled circles plus error bars show the more heavily binned Stokes parameters, which were calculated using the wavelength ranges listed in Table 2.

2.1.1. *Line and Continuum Polarization*

An important motivation for the spectropolarimetry of quasars is the ability to distinguish between the polarization of the continuum and that of the strong emission lines. In principle, this allows one to locate the polarizing medium with respect to the broad line region, as well as with respect to the much smaller continuum source. In practice, this separation is difficult due to the low signal-to-noise of the spectropolarimetry on faint objects. Results for PG 1632+706 and PG 2302+029 are shown in Table 3, where the line polarization is measured at the position of redshifted Lyman-α, and the continuum brackets the line. Table 3 also shows a comparison using a more extended region of continuum, given in the third line of Table 3 for each object, which gives a continuum polarization of better signal-to-noise. For PG 2302+029, this

FIG. 1.—Total intensity I, and the normalized Stokes parameters Q/I and U/I measured for the three quasars. The total intensity is binned by 2 pixels, and the dashed histogram shows the normalized Stokes parameters binned by 32 pixels. The filled circles show average values for the wavelength ranges listed in Table 2.

TABLE 2

ULTRAVIOLET POLARIZATION

Object	$\Delta\lambda$ (Å)	$Q/I \pm \sigma(Q/I)$	$U/I \pm \sigma(U/I)$	$p \pm \sigma(p)$[a]	$\theta \pm \sigma(\theta)$	Intensity[b] (ergs s^{-1} cm^{-2} $Å^{-1}$)
PG 1222+228.....	1994–2319[c]	0.0354 ± 0.0093	−0.0305 ± 0.0093	4.57 ± 0.93%	160 ± 6°	3.92×10^{-16}
	2224–2492[c]	0.0031 ± 0.0060	−0.0171 ± 0.0060	1.63 ± 0.60	140 ± 10	7.14×10^{-16}
	2493–2761[c]	0.0055 ± 0.0045	−0.0004 ± 0.0045	<0.90	~178	9.33×10^{-16}
	2762–3029[c]	0.0091 ± 0.0037	−0.0082 ± 0.0037	1.17 ± 0.37	159 ± 9	1.41×10^{-15}
	3030–3295[c]	0.0168 ± 0.0042	0.0019 ± 0.0042	1.64 ± 0.42	3 ± 7	1.67×10^{-15}
	2224–2761	0.0045 ± 0.0036	−0.0076 ± 0.0036	0.81 ± 0.36	150 ± 12	8.23×10^{-16}
	2762–3295	0.0133 ± 0.0028	−0.0027 ± 0.0028	1.33 ± 0.28	174 ± 6	1.55×10^{-16}
PG 1634+706.....	1990–2320[c]	0.0004 ± 0.0021	0.0029 ± 0.0021	<0.42	~41	1.17×10^{-14}
	2224–2492[c]	0.0034 ± 0.0020	0.0002 ± 0.0020	<0.40	~2	1.36×10^{-14}
	2493–2761[c]	0.0049 ± 0.0018	0.0009 ± 0.0018	0.46 ± 0.18	5 ± 10	1.34×10^{-14}
	2762–3029[c]	0.0024 ± 0.0016	−0.0017 ± 0.0016	<0.32	~163	1.90×10^{-14}
	3030–3295[c]	−0.0022 ± 0.0024	0.0034 ± 0.0024	<0.48	~61	1.19×10^{-14}
	2224–2761	0.0041 ± 0.0014	0.0006 ± 0.0014	0.39 ± 0.14	4 ± 9	1.35×10^{-14}
	2762–3295	0.0007 ± 0.0013	0.0003 ± 0.0013	<0.26	~11	1.55×10^{-14}
PG 2302+029.....	2224–2492[c]	0.0001 ± 0.0033	−0.0058 ± 0.0033	<0.66	~135	3.53×10^{-15}
	2493–2761[c]	−0.0009 ± 0.0029	−0.0106 ± 0.0029	1.02 ± 0.29	133 ± 8	3.53×10^{-15}
	2762–3029[c]	0.0031 ± 0.0032	−0.0023 ± 0.0032	<0.64	~162	3.09×10^{-15}
	3030–3295[c]	−0.0018 ± 0.0039	−0.0068 ± 0.0039	<0.78	~127	3.12×10^{-15}
	2224–2761	−0.0004 ± 0.0022	−0.0082 ± 0.0022	0.79 ± 0.22	134 ± 8	3.53×10^{-15}
	2762–3295	0.0006 ± 0.0025	−0.0046 ± 0.0025	<0.50	~139	3.10×10^{-15}

[a] Polarization values are corrected for low signal-to-noise bias.
[b] Mean intensity over wavelength range indicated.
[c] Wavelength range designated by horizontal bar in Figs. 1*a*–1*c*.

second comparison includes Lyman-α, C III and C IV in the line measurement, and the intervening regions were used for the continuum measurement.

The polarization values of the line and the line plus continuum are similar; and are consistent with the hypothesis that line and continuum have the same polarization. However, it is equally important to ask whether the hypothesis that the Lyman-α line is *unpolarized* is inconsistent with the data. In PG 1634+706, the Lyman-α equivalent width is 118 Å. If this line were unpolarized, its flux would dilute the polarization in the wavelength region of the line down to 0.09%. The line region in fact has a polarization of 0.23 ± 0.21%, so the hypothesis that the line is unpolarized cannot be ruled out. In PG 2302+029, the Lyman-α equivalent width is 71 Å. If that line were unpolarized, its flux would dilute the polarization in the wavelength region of the line down to 0.58%. The line region in fact has a *higher* polarization of 0.86 ± 0.31%, but the difference is not significant. If it is assumed that all three strong emission lines are unpolarized, the expected polarization of the summed line regions is 0.42%. This can be compared with the measured polarization of the summed line regions of 0.72 ± 0.23%, which again is not significantly different. No firm conclusion on whether or not the lines are polarized can be drawn from this data. A factor of two better signal-to-noise would be sufficient to make this determination.

2.1.2. *Circular Polarization*

Circular polarization has rarely been detected in the optical continuum of any active galaxy. A number of quasars show significant circular polarization at radio wavelengths (Komesaroff et al. 1984), where it is attributed to helical magnetic fields or anisotropic pitch angle distributions in a syn-

TABLE 3

LINE AND CONTINUUM POLARIZATION

Object	Regions	$Q/I \pm \sigma(Q/I)$	$U/I \pm \sigma(U/I)$	$p \pm \sigma(p)$	$\theta \pm \sigma(\theta)$	Intensity (ergs s^{-1} cm^{-2} $Å^{-1}$)
PG 1634+706.....	Line[a]	0.0025 ± 0.0021	−0.0019 ± 0.0021	0.23 ± 0.21%	161 ± 20°	2.67×10^{-14}
	Continuum[b]	0.0020 ± 0.0013	0.0013 ± 0.0013	0.20 ± 0.13	16 ± 16	1.33×10^{-14}
	Continuum[c]	0.0019 ± 0.0010	0.0014 ± 0.0010	0.21 ± 0.10	18 ± 12	1.30×10^{-14}
PG 2302+029.....	Line[d]	−0.0014 ± 0.0031	−0.0091 ± 0.0031	0.86 ± 0.31	131 ± 10	4.25×10^{-15}
	Continuum[e]	0.0008 ± 0.0029	−0.0083 ± 0.0029	0.78 ± 0.29	138 ± 10	3.07×10^{-15}
	Line[f]	−0.0008 ± 0.0023	−0.0075 ± 0.0023	0.72 ± 0.23	132 ± 9	3.72×10^{-15}
	Continuum[g]	0.0012 ± 0.0023	−0.0056 ± 0.0023	0.52 ± 0.23	141 ± 11	3.00×10^{-15}

[a] Wavelength range 2800–2900 Å (Lyman-α).
[b] Wavelength ranges 2500–2800 Å and 2900–3200 Å.
[c] Wavelength ranges 1900–2800 Å and 2900–3200 Å.
[d] Wavelength range 2400–2500 Å (Lyman-α).
[e] Wavelength ranges 2200–2400 Å and 2600–2800 Å.
[f] Wavelength ranges 2400–2600 Å, 2800–2900 Å and 3050–3200 Å (Lyman-α, C III, and C IV).
[g] Wavelength ranges 2200–2400 Å, 2600–2800 Å, 2900–3050 Å, and 3200–3300 Å.

chrotron source. Moore & Stockman (1981) set upper limits of 0.5% in the optical circular polarization in a number of blazars. Recently, Valtaoja et al. (1993) have quoted the marginal detection of circular polarization in two blazars. Over the past 20 years, though, very few high precision observations have been made.

The most sensitive test for circular polarization involves binning the entire spectrum to produce one number for a quasar. The results for the G270H observations were: $V/I = 0.0023 \pm 0.018$ (PG 1222+228), $V/I = -0.0005 \pm 0.0009$ (PG 1634+706), and $V/I = -0.0039 \pm 0.0016$ (PG 2302+029). Thus there is a marginal 2.4 σ detection for PG 2302+029, significant at the 98% confidence level if the errors are normally distributed.

Instrumental circular polarization in the FOS is no larger than 0.1% (R. Allen 1994, private communication) and the only way that spurious circular polarization can be generated in the data reduction is if the signal level is very low, which is not the case for any of these quasars. Splitting the spectrum into the same line and continuum regions described in the section above gives the following result. Circular polarization in the continuum is -0.45 ± 0.18%, but circular polarization in the wavelength region of the three strong lines is only -0.05 ± 0.18%. If this low level of circular polarization is real, it may be associated with the continuum of PG 2302+029.

2.1.3. *Is the Polarization Variable?*

It is important to determine whether or not the low level of polarization in these quasars is variable. Synchrotron polarization in strong radio sources is usually highly variable (Angel et al. 1978) because the emissivity reflects nonequilibrium conditions in a compact region of a relativistic jet (Blandford & Konigl 1979). By contrast, if polarization is caused by scatterers located beyond the broad line region, variations should have low amplitude and long timescales.

Berriman et al. (1990) published white light polarization measurements of PG 1222+228. The values were $p = 0.84 \pm 0.24$%, $\theta = 150 \pm 8°$ (1978), and $p = 1.07 \pm 0.28$%, $\theta = 143 \pm 8°$ (1979). WMSI published an R band measurement from 1984 March of $p = 0.82 \pm 0.20$%, $\theta = 147 \pm 7°$. There is no indication of variability in these three measurements. PG 1634+706 has not exceeded 0.5% in the two measurements from Berriman et al. (1990) and this paper, and the two measurements of PG 2302+029 from 1983 do not differ significantly. The data are sparse, but there is no evidence of the variability that is a hallmark of a nonthermal process for producing polarization.

2.2. *Notes on Individual Quasars*

2.2.1. *PG 1222+228 (Ton 1530)*

The *HST* flux levels in the total intensity spectrum are systematically lower by about 30% than those measured with *IUE*. Since the absolute flux calibration of the latter is more reliable, we have used the *IUE* points in our fitting. The highest frequency points drop below the level of the true continuum due to the merging of optically thick Lyman-limit absorbers below a rest wavelength of 912 Å. There is no evidence for near infrared variability in five observations made over a period of seven years (Neugebauer et al. 1989).

The most remarkable feature of the spectropolarimetry is the sharp rise in the degree of polarization of PG 1222+228 at the shortest wavelengths. As mentioned previously, instrumental polarization in the FOS is negligible at all ultraviolet wavelengths. Due to the low continuum level, it was necessary to verify that an appropriate value for the background was used in the reduction process, as the level of the background has a significant effect on the resultant values of linear polarization. The background must be subtracted off before Stokes parameters are fit to the modulated intensity measured through different orientations of the waveplate. If the background is either overestimated or underestimated, so is the polarization. The polarization in the bin from 1994 to 2319 Å was therefore calculated with three different assumptions for the background level. Since the background is electronic rather than astronomical, these experiments were carried out on the raw data in units of counts per pixel, and the results were converted into intensity units using the sensitivity function.

The FOS background is due to dark current in the Digicon detectors. It is measured periodically and shows little variation, except during passage through the South Atlantic Anomaly (when no science observations are made). The validity of the standard background was tested by considering the values of intensity, linear polarization, and polarization angle which were calculated after the subtraction of three different levels of background. The first was the standard value, which corresponds to a count rate of 0.0078 counts s^{-1} $pixel^{-1}$. As a minimum, zero background was assumed. As a maximum, it was assumed that all the signal in the bluest quarter of the G190H spectrum was background, corresponding to a count rate 0.011 counts s^{-1} $pixel^{-1}$. This is likely to be too high for a background level, since there is no evidence that the dark current varies by this much during normal science observations with the FOS. It is also likely that some of the signal from 1600–1800 Å is real continuum from the quasar. As evidence for this, the average intensity in the bluest quarter of the G190H spectrum of PG 1634+706, where the continuum is extinguished due to an optically thick intervening absorber, is only 0.0025 counts s^{-1} $pixel^{-1}$.

The results of this calculation are shown in Table 4. The systematic error on the derived polarization is given by the range under the assumption of minimum and maximum background levels. Even under the unrealistic assumption of zero background, the polarization only reduces to 2.7%. It was also possible to test for the rapid increase in polarization with the blue end of the data taken with the G270H grating. The polarization in the wavelength range 2381–2644 Å, redward of the Lyman limit system, is 0.85 ± 0.47%. The polarization in the narrow window 2224–2286 Å, blueward of the Lyman limit system, is 9.23 ± 2.64%. High ultraviolet polarization is seen in observations with two different gratings, and it is not an artifact of the assumed background level. The high extreme ultraviolet polarization of PG 1222+228 appears to be real.

PG 1222+228 was by far the highest redshift object in the sample, and similar increases in polarization at equivalent rest-wavelengths in the other two objects are not ruled out. The rise in polarization occurs near the position of a Lyman limit

TABLE 4

EXTREME ULTRAVIOLET POLARIZATION OF PG 1222+228

Background	Intensity (ergs s^{-1} cm^{-2} Å)	$p \pm \sigma(p)$	$\theta \pm \sigma(\theta)$
Maximum.....	$0.2914 \pm 0.0024 \times 10^{-15}$	5.74 ± 1.25%	$158.4 \pm 6°.1$
Standard	$0.3985 \pm 0.0024 \times 10^{-15}$	4.37 ± 0.91	157.7 ± 5.8
Zero	$0.6116 \pm 0.0024 \times 10^{-15}$	2.73 ± 0.59	158.4 ± 6.0

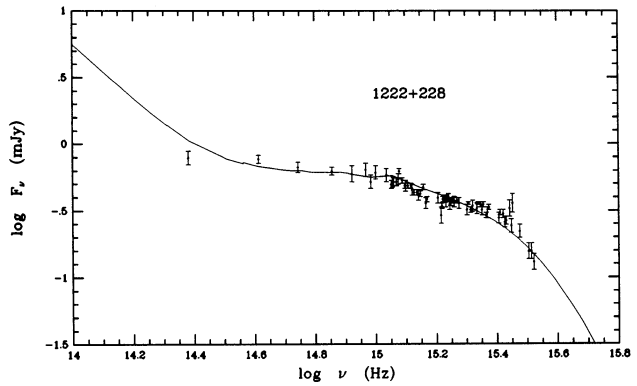

FIG. 2a

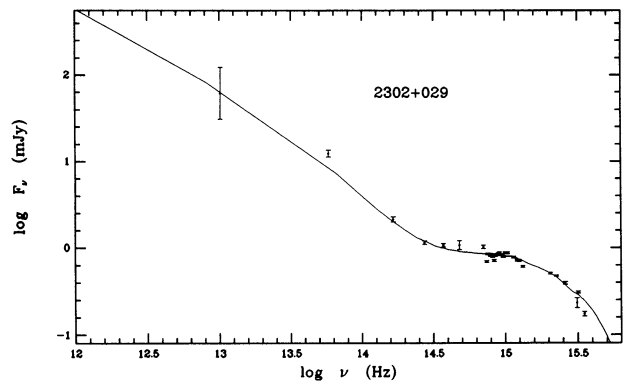

FIG. 2c

FIG. 2.—Spectral energy distributions for the three quasars. Log frequency vs. log flux density data points are shown with error bars. The multicomponent continuum fit, which includes thermal dust as a power law with an exponential cutoff at log $\nu = 14$, is shown as a solid line.

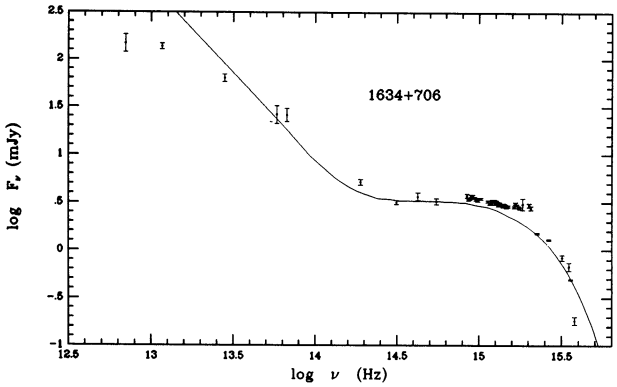

FIG. 2b

absorber at $z = 1.486$. There are absorbers at other wavelengths (where there is no increase in polarization), and the occurrence of the Lyman limit absorber at the wavelength where the polarization turns up may be a coincidence.

2.2.2. *PG 1634+706*

Since this quasar is nearly an order of magnitude brighter than the others, it has the most accurate polarimetry. This advantage is offset by the very low intrinsic polarization—generally less than 0.4%–0.05% at all wavelengths.

The total intensity flux spectrum is in good agreement with spectra from *IUE*, except that the higher SNR shows a richly populated Lyman-α "forest" blueward of the Lyman-α emission line. The 100 Å region of overlap between the G270H and G190H spectra shows excellent agreement. This quasar shows no evidence of variability at 2 μm (Neugebauer et al. 1989). Optical spectrophotometry, from Neugebauer et al. (1987) was not obtained simultaneously with the UV data, and shows a level $\sim$20% higher. Rather than artificially adjusted any data, in our model-fitting we have interpolated over this small discontinuity, which produces most of the residuals in the fit.

2.2.3. *PG 2302+029*

The *HST* total intensity spectrum for this quasar shows the worst disagreement with a previous *IUE* measurement, which is roughly constant 30% higher. Evidence that this is due to real variability comes from optical observations by Neugebauer et al. (1987), which show a level 40%–50% higher than the optical spectrophotometry we obtained with the Lick 3 meter telescope in 1987 August. Near infrared monitoring shows that this quasar has a more than 80% probability of being variable at 10 μm (Neugebauer et al. 1989). We have used the Lick optical spectrophotometry in our model-fitting, because it agrees well with the *IUE* data, which was also used.

3. MODEL FITTING AND RESULTS

3.1. *Continuum Fits and Component Fluxes*

The predictions of the different models for the origin of polarization require knowledge of the different continuum components contributing to the total flux. Therefore, we fit component flux models to the multiwavelength (infrared to ultraviolet) continuum energy distributions for each of the program quasars, following the procedures of WMSI. Given the high redshifts and high nonstellar luminosities, we are confident that the contamination by starlight below 3000 Å is less than 5% in each case.

The principal optical/UV component is assumed to be optically thick emission from an accretion flow. We described this blue thermal component with the thin disk models developed by Malkan (1983) and Sun & Malkan (1989). The fitted disk parameters, black hole mass and accretion rate, assuming zero inclination, are listed in Table 5. The long-wavelength ($\lambda \geq 1$ μm) continuum, as would be appropriate for thermal emission, is fitted with a power law with high-frequency cutoff around $\lambda = 3$ μm (see Malkan 1991 and discussion in § 4.2 of WMSI). The continuum at rest wavelengths of 2500–3700 Å) is contaminated by contributions from the broad emission line region (mostly a blend of Balmer continuum and Fd II line emission). An estimate of this component is included in our fits. Figures 2*a*–2*c* show the continuum fits with a thermal infrared continuum.

3.2. *Polarization Model Fitting*

Each of the quasar's observed polarization spectra were fit with seven possible models for the origin of the polarization: a power-law synchrotron emitter, three types of scattering due to dust, a nonspherical distribution of electrons scattering all of the nuclear light, electron scattering of the blue thermal component, and transmission through grains in the host galaxy. These polarized flux fits are illustrated in Figure 3*a*–*c*. The results of a χ^2 calculation showing which models best fit the data are given in Table 6, and Table 7 gives the flux by component in each waveband.

Our new results confirm several conclusions made by WMSI about quasar polarization. The absence of any wavelength-

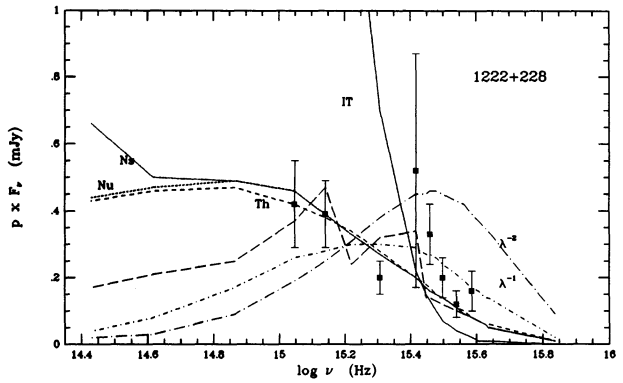

FIG. 3*a*

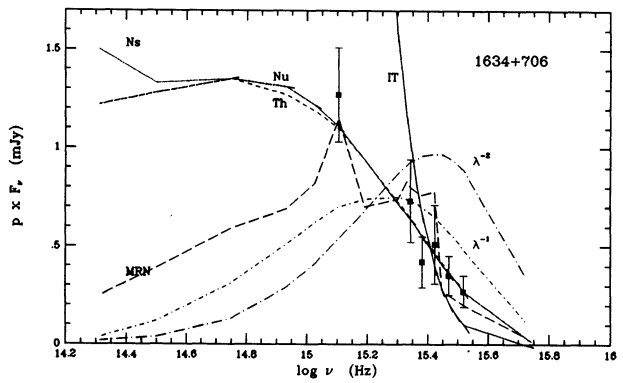

FIG. 3*b*

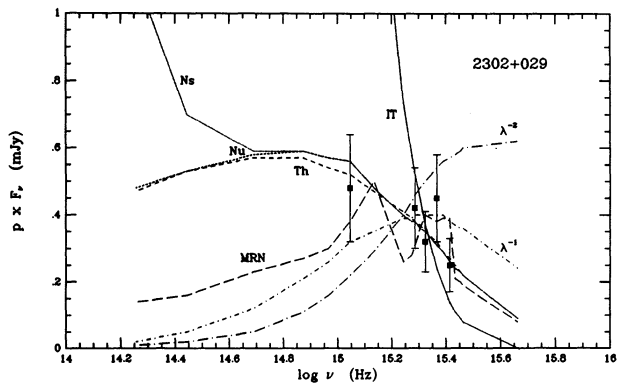

FIG. 3*c*

FIG. 3.—Polarized continuum fluxes for the three quasars. Ultraviolet data points from Hubble Space Telescope observations, optical data includes published *U*, *B*, *V*, *R*, and *I* and white light (unfiltered) measurements where available, with error bars. Polarization models are shown with different line types and are named with symbols and abbreviations defined in the text.

dependence of polarization position angles is consistent with WMSI's findings. In no case can the polarizations be produced by transmission through aligned dust grains (the "IT" hypothesis). The peaked polarization described by the Serkowski law does does not match the observations of any quasar. We have also considered polarization from small dust grains, with scattering cross sections proportional to λ^{-1} or λ^{-2}. These models are not among the best three fits for any of the three quasars. There is better agreement with the predicted polarization produced by dust scattering obeying the "MRN" relation used by WMSI to describe normal interstellar grains (Mathis et al. 1977, hereafter MRN).

Another possible source of polarization is a nonthermal power law (e.g., synchrotron emission). However, nonthermal emission could not produce much of the observed flux at all wavelengths, because our multiwavelength continuum fits do not reproduce a power law with such a flat slope. Also, there is no evidence for the large amplitude variability that is usually associated with blazar emission (Neugebauer et al. 1989). The possible exception is PG 1634+706. Its spectrum in the UV range we observed happens to be rather steep ($F_\nu \propto \nu^{-1.4}$); therefore, the constancy of observed polarization with wavelength results in an unusually steep drop in polarized flux with wavelength, which could be consistent with the presence of a weak blazar (as WMSI found for PG 1048−09 = 3C 246). This steep rise of polarization to longer wavelengths in PG 1634+706, a radio-weak object, could probably be ruled out by optical or infrared polarimetry.

Excellent fits to the data are provided for all objects by the "Nonstellar," "Nuclear," and "Thermal" models, and acceptable fits are provided by the "MRN" dust model. The three most favored explanations for the quasar polarizations all require some kind of electron scattering of the nuclear continuum, which we discuss next.

4. DISCUSSION

The WMSI broadband optical polarimetry study narrowed the permitted models for the origin of polarization in AGNs to

TABLE 5

COMPONENT FITTING PARAMETERS

Object	σ_{PL}	S_{PL}(5400 Å) (mJy)	S_B(3646 Å) (mJy)	*BH* Mass ($M_\odot$ yr^{-1})	Accretion Rate ($M_\odot$ yr^{-1})
PG 1222+228.....	−1.30	0.17	0.02	6.0×10^9	29.0
PG 1634+706.....	−1.10	0.50	0.10	13.0×10^9	60.0
PG 2302+029.....	−1.60	0.14	0.05	3.2×10^9	11.6

TABLE 6

POLARIZATION HYPOTHESES—REDUCED χ^2-VALUES

Object	Nonstellar	Nuclear	Thermal	MRN	λ^{-1}	λ^{-2}	IT
PG 1222+228.....	1.45	1.45	1.43	2.33	2.15	18.0	260
PG 1634+706.....	0.34	0.34	0.37	2.11	4.38	24.2	135
PG 2302+029.....	0.43	0.43	0.37	1.45	1.32	6.49	50.2

1995ApJ...440...80I

TABLE 7

COMPONENT FLUXES—FRACTION OF TOTAL FLUX

AGN	Component	0.133 (μm)	0.211 (μm)	0.212 (μm)	0.226 (μm)	0.236 (μm)	0.249 (μm)	0.263 (μm)	0.290 (μm)	0.303 (μm)	0.316 (μm)	*U* 0.325 (μm)	*B* 0.350 (μm)	*V* 0.451 (μm)	*R* 0.551 (μm)	*I* 0.661 (μm)	*J* 0.820 (μm)	*H* 1.25 (μm)	*K* 2.21 (μm)	*L* 3.4 (μm)
1222+228.....	Stars	0.02	<0.01	<0.01	<0.01	<0.01	<0.01	<0.01	<0.01	<0.01	<0.01	<0.01	<0.01	<0.01	<0.01	<0.01	<0.01	0.01	0.09	0.16
	Power	<0.01	<0.01	<0.01	<0.01	<0.01	<0.01	<0.01	<0.01	<0.01	<0.01	<0.01	<0.01	<0.01	<0.01	<0.01	<0.01	<0.01	0.02	0.12
	Thermal	0.98	>0.99	>0.99	>0.99	>0.99	>0.99	>0.99	>0.99	>0.99	>0.99	>0.99	>0.99	>0.99	0.99	>0.96	0.89	0.93	0.85	0.68
	Recomb	<0.01	<0.01	<0.01	<0.01	<0.01	<0.01	<0.01	<0.01	<0.01	<0.01	<0.01	<0.01	<0.01	0.01	0.04	0.11	0.06	0.05	0.04
1634+706.....	Stars	<0.01	<0.01	<0.01	<0.01	<0.01	<0.01	<0.01	<0.01	<0.01	<0.01	<0.01	<0.01	<0.01	<0.01	<0.01	<0.01	0.01	0.05	0.06
	Power	<0.01	<0.01	<0.01	<0.01	<0.01	<0.01	<0.01	<0.01	<0.01	<0.01	<0.01	<0.01	<0.01	<0.01	<0.01	<0.01	<0.01	0.03	0.18
	Thermal	>0.99	>0.99	>0.99	>0.99	>0.99	>0.99	>0.99	>0.99	>0.99	>0.99	>0.99	>0.99	>0.99	0.98	0.97	0.96	0.98	0.91	0.75
	Recomb	<0.01	<0.01	<0.01	<0.01	<0.01	<0.01	<0.01	<0.01	<0.01	<0.01	<0.01	<0.01	0.01	0.02	0.03	0.04	0.01	0.01	0.01
2302+029.....	Stars	<0.01	<0.01	<0.01	<0.01	<0.01	<0.01	<0.01	<0.01	<0.01	<0.01	<0.01	<0.01	<0.01	<0.01	<0.01	0.01	0.07	0.17	0.14
	Power	<0.01	<0.01	<0.01	<0.01	<0.01	<0.01	<0.01	<0.01	<0.01	<0.01	<0.01	<0.01	<0.01	<0.01	<0.01	<0.01	0.02	0.19	0.49
	Thermal	>0.99	>0.99	>0.99	>0.99	>0.99	>0.99	>0.99	>0.99	>0.99	>0.99	>0.99	>0.99	0.96	0.91	0.93	0.94	0.88	0.62	0.36
	Recomb	<0.01	<0.01	<0.01	<0.01	<0.01	<0.01	<0.01	<0.01	<0.01	<0.01	<0.01	<0.01	0.04	0.09	0.06	0.04	0.03	0.02	0.02

essentially two: dust scattering or electron scattering of the nonstellar nuclear continuum. The UV polarization is either flat or declining with frequency in two of the three quasars, PG 1634+706 and PG 2302+029. Dust scattering models, which predict increased polarization with frequency, do not give as good fits to the data as models which predict flat or declining polarization with frequency.

4.1. *Interpreting the Polarized Flux Spectrum*

Since the polarizations from optical to UV wavelengths tend to be flat, the slope of the polarized flux spectrum is very similar to the slope of the total intensity spectrum—an average slope is $p_\nu \times F_\nu = k \times \nu^{-0.8\pm0.5}$. In view of the wavelength-independent position angle, it is simplest to attribute this polarized flux to a single continuum component. One possibility is that most of the continuum we observe in the UV comes from a single physical component (but not a power law), which has a low, approximately wavelength-independent polarization at wavelengths longer than 800 Å. Indeed, WMSI fitted the rest-UV ($\lambda < 3000$ Å) continuum primarily with a single component which has the spectral shape of optically thick thermal emission. Since this thermal continuum is the dominant continuum component in the UV flux, it may be surprising that the "Thermal" hypothesis gives some of the smallest χ^2 values. However, this model only gives a good fit because the polarization is independent of wavelength.

The success of the "Thermal" hypothesis fits does not prove that the UV continuum is thermal emission, nor does it prove it arises in an accretion disk. It *does* prove that if the UV is disk light, it has a very small, nearly wavelength-independent polarization (of course, this is true for any single component causing the polarization). Yet another possibility, the "Nonstellar" hypothesis, is that *all* of the nuclear continuum is uniformly polarized (perhaps by electron scattering). This hypothesis is only distinguishable from the "Thermal" hypothesis at wavelengths where the thermal component is *not* the dominant flux contributor—i.e., in the red. This is why the model curves predicting polarized flux from the "Nonstellar" and "Thermal" models overlap throughout the rest-UV wavelengths which we observed. The predictions of these two models deviate in the observed infrared, where a standard thin accretion disk would no longer produce all of the observed flux. The nonstellar hypothesis predicts greater polarization in the infrared than does the thermal model.

The only difference between the "Nuclear" and "Thermal" models is that the former has unpolarized BLT emission. This only has a significant effect at rest wavelengths around 3800–2300 Å, which is too small to make a significant difference to the χ^2 values in Table 6.

4.2. *Interpreting the Far-UV Polarization of PG 1222+228*

Figure 4 shows the wavelength dependent polarization of 1222+228 (Ton 1530), where the data in the overlap region of the G190H and G270H gratings has been combined into a weighted average. The sharp rise in polarization is clear when the data is compared to three simple models, with polarization independent of wavelength, increasing as λ^{-1} and increasing as λ^{-4}. If the far-UV continuum is emitted from a standard thin accretion disk, with surface temperature proportional to $r^{-3/4}$, higher-frequency photons tend to originate from smaller radii. Nonetheless due to the finite width of the Planck function, the total disk flux at a given frequency must have significant contributions from a range of annuli. The contributions of these annuli to the total flux at nearby frequencies cannot be dramatically different. To take an extreme case, suppose that the increase in polarization at shorter wavelengths were due to the increasingly dominant flux contribution made by the (highly polarized) inner region of an accretion disk. Could the observed sudden rise in polarization be explained by an inner disk region with *wavelength-independent* polarization? A calculation shows that the observed change—polarization *at least* doubles while frequency changes by no more than 20%—is too sudden. Consider a simplified disk model in which effective temperature goes as $r^{-3/4}$. Then the integrated disk flux out to a radius where the temperature drops to T_b is proportional to the integral $(\int_0^{X_b} x^{5/3}\,dx)/(e^x - 1)$, where the upper boundary of the integral, X_b, is $h\nu/kT_b$.

The best possible case would be when the polarization in the disk outside of this boundary drops immediately to zero. We must then ask whether or not the value of the definite integral can increase by a factor of two (or more) when X_b increases by only 20% (corresponding to a 20% increase in observing frequency)? A numerical integration of this integral over a wide range of values of X_b shows that the answer is always no. The largest percent changes in the integral occur for small values of X_b, where we can approximate the integral by $(3/5)X_b^{5/3}$. Even in this most favorable case, a 20% increase in X_b only increases the integral by 36%, far short of the 100% increase required. Relativistic effects in a more sophisticated accretion disk model do not appear to be large enough to alter this result. We therefore conclude that if the observed rise in polarized far-UV flux originates in an accretion disk, the

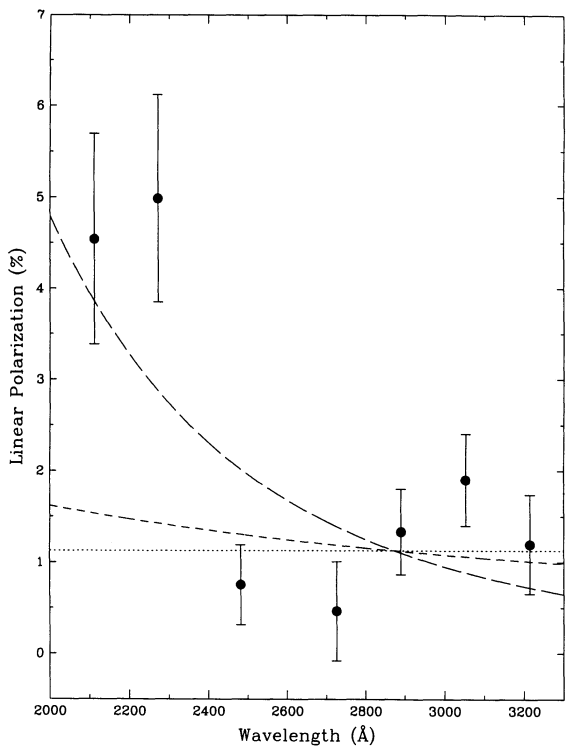

FIG. 4.—Wavelength dependence of the linear polarization of PG 1222+228, using data from both G190H and G270H gratings. Polarization values are calculated using evenly divided wavelength bins for each grating. Simple models, normalized at the mean wavelength and polarization of the G270H data, show no wavelength dependence (*dotted line*), $p \propto \lambda^{-1}$ (*short-dashed line*), and $p \propto \lambda^{-4}$ (*long-dashed line*).

region where it is produced cannot generate wavelength-independent polarization. This inner region of the disk would have to produce polarization which increases with frequency. To produce this intrinsic increase in polarization would probably require that some scattering process, such as Thomson or Compton scattering, becomes dominant at shorter wavelengths.

4.3. *Possible General Relativistic Effects*

By symmetry, the intrinsic polarization from an accretion disk should be either perpendicular or parallel to the disk's polar rotation axis projected onto the sky; the details depend on the temperature and surface structure of the disk (Webb & Malkan 1986; Coleman & Shields 1990). It has also long been realized (Conners, Piran, & Stark 1980) that if polarized emission arises near a black hole, the electric field position vector will be rotated as the light propagates through the strong gravitational field. This general relativistic effect will only affect photons emitted from within a few tens of gravitational radii. If higher frequency continuum photons originate closer to the black hole, the polarization should *rotate* with frequency, especially if the hole is spinning rapidly.

Our spectropolarimetry sets an empirical limit of 6° on the rotation of the polarization vector. If we adopt the thin disk models fitted in § 4, this limit is significant, especially for PG 1222+228 which has polarimetry extending all the way down to rest wavelengths of 700–800 Å. We use the calculations of Laor, Netzer, & Piran (1990) to transform our thin accretion disk fits to the average viewing angle of $\cos i = 0.5$ (a disk viewed face-on would not be expected to show any polarization), enabling a direct comparison with their Figures 1–4. As described in equations (2) and (3) of Sun & Malkan (1989), for the rapidly spinning (Kerr) hole our fitted black hole masses (which assumed a face-on disk) must be increased by a factor of 4, while the physical accretion rate hardly changes. To transform to a nonrotating (Schwarzschild) hole viewed at $\cos i = 0.5$, our tabulated black hole masses must be tripled, and the mass accretion rates must be increased by a factor of 4. Note that for $\cos i = 0.5$, the inferred accretion rates, for either Kerr or Schwarzschild holes, are 11%–17% of the Eddington limit for these quasars.

If we first assume a Schwarzschild hole, the predicted rotations of the polarization vector in PG 1222+228 are 6° in the shortest wavelength bin measured (an observed wavelength of 2156 Å), and 4° in the near-UV bin centered on 3029 Å. These small rotations are consistent with our data, within the observational uncertainties. However, for a rapidly rotating hole, the predicted polarization position angle changes are 22° at 3029 Å and 32° at 2156 Å, which are strongly ruled out by the data. The position angles in PG 1634+706 have large measurement errors, but in PG 2302+029 the position angle is measured accurately down to a rest wavelength of 1290 Å. Even to this redder limit, the predicted polarization rotation of 15 degrees for the extreme Kerr black hole can be ruled out. The smaller position angle rotation of 4° predicted for a Schwarzschild hole cannot be ruled out. Although these predictions were made for an accretion disk with a local blackbody spectrum, Laor et al. (1990) predict almost as large changes in position angle when they replace the local blackbody spectra with simple atmosphere models.

The conclusion that the Kerr models predict a larger polarization rotation than we observe is not sensitive to the assumed inclination of the disks. Roughly speaking this is because the radius from which the observed UV photons arise, in units of the gravitational radius, increases only mildly as the disk inclination increases. In edge-on disks, the far-UV continuum comes from a larger number of gravitational radii (i.e., where the gravitational potential is weaker). However, this effect is mostly offset by the fact that the relativistic polarization rotations are enhanced for a nearly equatorial observer. The observed limits on position angle rotations at short rest wavelengths in PG 1222+228 (and to a lesser extent PG 2302+029) permit interesting speculations within the context of the standard model of accretion onto a supermassive black hole. Either the far-UV continuum arises from more than a few tens of gravitational radii, or the black hole is not spinning rapidly, or the black hole is less massive than predicted by the standard model.

5. CONCLUSIONS

None of the three observed quasars showed wavelength dependence of the strength or position angle of the polarization from optical wavelengths down to a rest wavelength of 800 Å (over two octaves in frequency). This behavior strongly suggests an electron scattering origin for the low level polarization, but it is not clear whether these scatterers are intrinsic to the continuum-emitting region or well outside it. The signal-to-noise of the measurements is insufficient for us to determine if the broad emission lines are polarized or not. There is some evidence for circular polarization of the continuum in PG 2302+029, although it is only significant at the 98% confidence level.

The levels of ultraviolet polarization are similar to or slightly lower than the previously-measured levels of optical polarization. There is no evidence for variable polarization, such as would be expected from a compact synchrotron source. The polarized flux spectra are flat with a typical slope $pF_\nu \propto \nu^{-0.8\pm0.05}$. Unlike the case of several high luminosity Seyfert 1 nuclei studied previously, polarization caused by scattering from dust grains does not provide the best fit to the polarization spectra of these luminous quasars. The hypothesis that the polarization in these quasars is produced by transmission through aligned interstellar grains in the Milky Way or the host galaxy appears to be ruled out. The spectra are consistent with a wavelength independent polarization proportional to the total nonstellar light or, possibly, to the contribution of the blue thermal component.

An increase in UV polarization shortward of a rest wavelength of 800 Å has been observed in PG 1222+228 at the 4 σ significance level. This sharp rise is not attributable to any known instrumental artifact. Although the rise occurs near an opacity edge due to an intervening Lyman limit absorber, this is most likely a coincidence. Assuming that the far UV emission comes from an accretion disk, the rapid polarization rise cannot be produced by any intrinsic process that is wavelength independent. Even if the inner regions of the accretion disk are highly polarized, measurements at any UV wavelength include emission from a range of annuli, which limits the slope of the wavelength dependence of polarization. A scattering process other than electron scattering must become important at high frequencies. It is noted, however, that the scattering geometry of the new mechanism must be similar since there is no rotation of the polarization position angle at high frequencies.

Assuming the standard paradigm of an accretion disk surrounding a supermassive black hole, observations of PG 1222+228 at short rest wavelengths allow a search for an effect

predicted by strong field general relativity. Taking reasonable estimates of black hole mass and disk inclination, the expected position angle rotation of 20 degrees at the highest frequencies is not observed. Such a result could be explained by a black hole which is not rotating rapidly or is less massive than predicted by the standard model, or it could be explained by high frequency emission which originates from more than a few tens of gravitational radii from the black hole.

We are grateful to Rich Allen, for diligent and patient assistance with the polarization reduction software, and to Paul Smith for polarimetric insights. Support for this work was provided by NASA through GO Program grant numbers 2524 and 3732 from the Space Telescope Science Institute, which is operated by the Association of Universities for Research in Astronomy, Inc., under NASA contract NAS 5-26555.

REFERENCES

Allen, R. G., & Angel, J. R. P. 1982, in Proc. SPIE, Instrumentation in Astronomy IV, 331, 259
Allen, R. G., & Smith, P. S. 1992, FOS IDT Report CAL/FOS-078
Allen, R. G., et al. 1993, ApJ, 403, 610
Angel, J. R. P., et al. 1978, in Pittsburgh Conf. BL Lac Objects, ed. A. M. Wolfe (Pittsburgh: Univ. Pittsburgh), 117
Antonucci, R. 1992, in Testing the AGN Paradigm, ed. S. Holt, S. Neff, & M. Urry (New York: AIP), 486
———. 1993, ARA&A, 31, 473
Berriman, G., Schmidt, G. D., West, S. C., & Stockman, H. S. 1990, ApJS, 74, 869
Blandford, R. D., & Konigl, A. 1979, ApJ, 232, 34
Bregman, J. N. 1990, Astron. Astrophys. Rev., 2, 125
Burstein, D., & Heiles, C. 1978, ApJ, 225, 40
Cimatti, A., di Serego Alighieri, S., Fosbury, R. A. E., Salvati, M., & Taylor, D. 1983, MNRAS, 264, 421
Coleman, H., & Shields, G. 1990, ApJ, 363, 415
Connors, P. A., Piran, T., & Stark, R. F. 1980, ApJ, 235, 224
Impey, C. D., & Neugebauer, G. 1988, AJ, 95, 307
Kellerman, K. I., Sramek, R., Schmidt, M., Shaffer, D. B., & Green, R. 1989, AJ, 98, 1195
Komesaroff, M. M., et al. 1984, MNRAS, 208, 409
Landau, R., et al. 1986, ApJ, 308, 78
Laor, A., Netzer, H., & Piran, T. 1990, MNRAS, 242, 560
Malkan, M. 1983, ApJ, 268, 582
———. 1989, Theory of Accretion Disks, ed. F. Meyer et al. (Dordrecht: Kluwer), 19
———. 1991, Physics of Active Galactic Nuclei, ed. S. Wagner & W. Duschl (Dordrecht: Kluwer), 109
Malkan, M., & Sargent, W. L. W. 1982, ApJ, 254, 22
Mathis, J. S., Rumpl, W. M., & Nordsieck, K. H. 1977, ApJ, 217, 425 (MRN)
Mead, A. R. G., et al. 1990, A&AS, 232, 606
Miller, J., & Goodrich, R. 1990, ApJ, 355, 456
Moore, R. L., & Stockman, H. S. 1981, ApJ, 243, 60
Neugebauer, G., Green, R. F., Matthews, K., Schmidt, M. Soifer, B. T., & Bennett, J. 1987, ApJS, 63, 615
Neugebauer, G., Soifer, B. T., Matthews, K., & Elias, J. H. 1989, AJ, 97, 957
Stockman, H. S., Moore, R. L., & Angel, J. R. P. 1984, ApJ, 279, 584
Sun, W. H., & Malkan, M. A. 1989, ApJ, 346, 68
Tran, H., Miller, J., & Kay, L. 1992, Testing the AGN Paradigm, ed. S. Holt, S. Neff, & M. Urry (New York: AIP)
Valtoaja, L., Karttunen, H., Valtaoja, E., Shakhovskoy, N. M., & Efimov, Yu. S. 1993, A&A, 273, 393
Wardle, J. F. C., & Kronberg, P. P. 1974, ApJ, 194, 249
Webb, W., & Malkan, M. 1986, The Physics of Accretion onto Compact Objects, ed. K. O. Mason, M. G. Watson, & N. E. White (Berlin: Springer), 15
Webb, W., Malkan, M., Schmidt, G., & Impey, C. 1993, ApJ, 419, 494 (WMSI)